The 5th Joint International Conference on Multibody System Dynamics
June 24 – 28, 2018, Lisboa, Portugal

TerRA: Terramechanics for Real-time Application

Stefan Barthelmes[1]
[1] *Institute of System Dynamics and Control, German Aerospace Center (DLR), Stefan.Barthelmes@dlr.de*

ABSTRACT — *Wheeled mobile robots are popular in planetary exploration and other challenging applications due to their robustness and energy-efficient mobility. Simulation models of such robots have gained importance for both, the development and model-based controller and observer design. The most challenging part to model is the interaction between soil and wheels - called Terramechanics. Although models for that interaction exist, they either have shortcomings in certain effects that are important for the locomotion or are computationally expensive.*
In this work, the novel empirical model 'Terramechanics for Real-Time Application (TerRA)' for normal and longitudinal force calculation is presented, which is developed specifically for the locomotion of wheeled mobile robots in sandy terrain. It includes an elasto-plastic normal force, plastic and dynamic sinkage as well as a longitudinal force that is calculated dependent on the history of slip and velocity. By circumventing any spatial discretization, the computational effort of TerRA is low enough to make it suitable for rover optimization and on-board application.

1 Introduction

Mobile systems in planetary surface exploration are mostly wheeled rovers as they have proven to be robust and at the same time relatively simple in design and operation. The most prominent examples are NASA/JPL's Mars Exploration Rovers (MER) 'Spirit' and 'Opportunity' [1, 2] and their most recent Mars Science Laboratory (MSL) mission with the rover 'Curiosity' [3]. Despite the missions being extremely successful, difficulties in the locomotion on soft sands were experienced several times: Spirit got stuck in the sands of Troy on sols 1871 to 1899 after experiencing extensive unexpected slip, leading to high slip and sinkage [1]. Opportunity only barely escaped a sand field after about 20 sols of over 98.9% average slip [2, 4] on sols 463-483 on Purgatory dune. Even Curiosity developed too much slip in hidden valley on sols 706 to 713, needed to be backed out and a decision was made to avoid sand ripples in future drives where possible [5].

Understanding, predicting and reacting to the terramechanics on soft soil is therefore of high importance for designing and operating planetary exploration rovers. A wide variety of models can hence be found in the literature ranging from computationally expensive but high fidelity discrete element methods to one-point empirical models [6]. When it comes to models that are suitable for a full rover simulation in a reasonable time frame, most publications are based on the work of BEKKER, WONG, JANOSI & HANAMOTO [7], a good overview of these approaches can be found in [8]. Many researchers have shown shortcomings of said BEKKER based models and proposed additional equations and/or parameters to overcome them, e.g. the impact of the wheel width [9], slip-sinkage [10, 11], grouser force and sidewall resistance [11]. Different angles of maximum normal and shear stress plus three parameters for skid-sinkage are introduced in [12] while [13] presents a different approach for the normal and shear stress calculations. All said approaches are based on normal and shear stress calculation necessitating a subsequent integration over the contact patch which reveals the directions of normal and shear forces but makes the model more computationally expensive than pure one-point force calculations. The real-time capability is approached with simplifications to get a closed form in [14] and [15]. Few different approaches can be found in the literature, e.g. a hypervolumetric approach in combination with common continuous soil models [16] or an alternative to a finite-element approach with an elasto-plastic constitutive relation and a velocity-field requiring meshing of the wheel surface [17]. Both said approaches ranged close to real-time capability according to the respective authors.

The approach of this work is the development of a novel empirical one-point model due to said problems that have been documented. Within this work, only the longitudinal wheel direction is considered while lateral forces and turning torques shall be developed in future work. In TerRA, observed functional dependencies are covered and incorporated from the beginning and parameters allow to fit the model to a certain wheel-soil combination. For application in onboard controllers or observers as well as in rover optimization, one crucial aspect of TerRA is computation time. To be suitable for future use on onboard hardware, TerRA must be multiple times faster than real-time on the standard office PC that is used within this work.

More details on the desired effects as well as modeling requirements can be found in Section 2. The derivation of the model is shown in Section 3 and results follow in Section 4. In Section 5, the work is concluded and remarks on future work are given.

2 Model requirements

Due to the shortcomings of existing terramechanics models (cf. Section 1), TerRA was developed as a new empirical model. To make sure that the model suits its purpose and to allow for a structured development, modeling principles and effects to be modeled are given in Section 2.1 and Section 2.2, respectively.

2.1 General requirements

Two general requirements to be met with the model are formulated in this section.

- The model parameters of TerRA should be constant for a certain wheel-soil combination, i.e. after fitting the model with a set of scenarios, it should ultimately be able to interpolate and extrapolate to other scenarios. However in this work only the development and tuning procedure is shown, while the validation is subject to future work.
- To ensure the best possible computational efficiency, any spatial discretization of the soil or the wheel contact patch shall be avoided.

2.2 Terramechanical effects

The overall goal for TerRA regarding terramechanical effects is to model the forces of the wheel-soil contact. Besides correct steady-state behavior, some dynamic effects that are important for the locomotion need to be captured as well within the capabilities of a one-point model. To meet these goals, the following required effects were selected beforehand:

Plastic sinkage of a wheel results from a plastic deformation of sandy soil. When a wheel is pushed or dropped into sand, plastic sinkage occurs, i.e. this sinkage does not decrease anymore unless the wheel moves translationally and thereby drives out of the area of plastic sinkage. Although a memory of the plastic soil deformations for preceding wheels, i.e. multi-pass, is not feasible without a spatial soil discretization, the plastic sinkage behavior shall still be covered for the individual wheels.

Slip-sinkage is a dynamically rising sinkage that develops with wheel slippage and is crucial since it can lead to embedding. Especially grousered wheels dig into the soil when slipping which leads to a higher soil resistance but not a higher normal force since the soil is removed rather than compacted by the slippage. The effect of the compaction rising with the depth that naturally layered sands show is omitted herein.

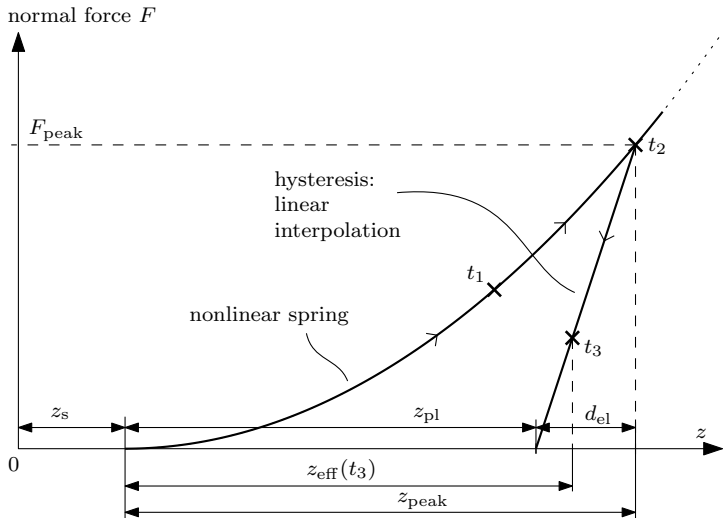

Fig. 1: Normal force as a function of sinkage.

Slip and traction force are highly correlated, however compared to on-road tire modeling a direct relationship between the two cannot be stated. The traction force is rather dependent on the soil shear history which - similar to the plastic sinkage - cannot be explicitly modeled without a spatial discretization including soil memory. Despite this fact, soil loading within one wheel-soil contact shall still be approximated, i.e the traction force development depends on the shearing history of the soil. The resulting slip of one wheel shall hence develop dynamically and converge to a certain value which is dependent on wheel load, soil and external forces such as downhill force.

Resistance force of the soil is dependent on wheel sinkage and can ultimately lead to the wheel getting stuck. Naturally, the resistance force can only counteract the traction force and cannot lead to a positive acceleration.

Convergence to a stable, reproducible state shall be achieved for constant external conditions. Despite the dynamic behavior, this convergence in the states - e.g. slip, sinkage - must be achieved after a certain transient phase.

3 Model development

In this section the details of the normal and tangential force models are derived in Sections 3.1 and 3.2, respectively.

3.1 Normal direction

The normal force calculation in TerRA is penetration-based with an elasto-plastic model that was inspired by the work of [18] for the HP^3 Mole, a self-impelling nail. For wheeled locomotion, additional sinkage computations are needed to achieve the effects that were required in Section 2.2. A division of the total sinkage to allow for slip-sinkage is introduced in Section 3.1.1, a hysteresis is derived in Section 3.1.2 for plastic soil deformation and the modeling of the dynamic sinkage is detailed in Section 3.1.3.

3.1.1 Effective and non-effective sinkage

To achieve a slip-sinkage that does not influence the normal force, the full penetration from the multibody simulation z is divided into two portions (see Fig. 1):

- *Effective sinkage* (z_{eff}): This is the sinkage that is used for the normal force calculation. Note that it contains a *plastic* sinkage z_{pl}.

- *Slip-sinkage* (z_s): This sinkage is built up by slippage of the wheel and does not lead to rising normal force. It can be thought of as soil that is removed from beneath the wheel (e.g. by grousers). Due to the soil being physically moved and the inhomogeneity of the soil compaction over depth being omitted, the slip-sinkage does not add to the normal force.

Both sinkages add up to the total geometric sinkage z as

$$z = z_{\text{eff}} + z_s. \tag{1}$$

3.1.2 Hysteresis for plastic deformation and damping

In Fig. 1, the different sinkages are visualized in a force vs. sinkage diagram. This part of TerRA is a standard elasto-plastic model as it was used for sand modelling in [18] with a nonlinear spring characteristic. The nonlinear peak spring force is calculated as

$$F_{\text{peak}} = k_c z_{\text{peak}}^{(k_{\text{exp}})} \tag{2}$$

from the peak sinkage z_{peak} with the spring constant and exponent k_c and k_{exp}. To ensure that the soil shows plastic behavior, a hysteresis with an elastic layer of thickness d_{el} is introduced and a linear regularization of the spring force is performed as

$$F_{\text{spring}} = k_{\text{el}} \left(z_{\text{eff}} - z_{\text{pl}} \right). \tag{3}$$

Therein the plastic sinkage is defined as

$$z_{\text{pl}} = z_{\text{peak}} - d_{\text{el}} \tag{4}$$

with the elastic layer of thickness d_{el} having a fixed stiffness k_{el},

$$d_{\text{el}} = \frac{F_{\text{peak}}}{k_{\text{el}}}. \tag{5}$$

The idea becomes clearer when following the three marked times in Fig. 1 for a wheel that is dropped on the soil without a rotation: At time t_1, the sinkage is rising and the normal force develops according to its nonlinear dependency (Eq. (2)). At time t_2, the wheel has reached its maximum sinkage and would normally be pushed out again following the nonlinear spring characteristics. Instead of this elastic behavior, the maximum sinkage z_{peak} is kept at its current value when the penetration velocity changes sign, since soil mainly deforms plastically. At time t_3, the wheel finds its equilibrium within the defined elastic layer d_{el}, keeping the plastic sinkage z_{pl}.

Additional to the spring force from Section 3.1.2, a linear undercritical damping force with the damping ratio $k_d < 1$ is introduced as

$$F_{\text{damp,n}} = k_d 2\sqrt{k_c m} \cdot \max\left(\dot{z}_{\text{eff}}, 0\right). \tag{6}$$

for positive effective sinkage gradients $\dot{z}_{\text{eff}}$ with a mass estimate m and the damping factor k_d. The total normal force is the sum of spring and damping force,

$$F_n = F_{\text{spring}} + F_{\text{damp,n}}. \tag{7}$$

3.1.3 Dynamic sinkage

In the literature, dynamic sinkage in models without soil discretization is commonly modeled as a linear slip-dependency of the exponent of the sinkage in the normal stress calculation [10, 11]. Since a differentiation between effective and non-effective slip-sinkage is made in this work, the latter is calculated explicitly.

The dynamic sinkage is composed of an inward and an outward sinkage velocity, $\dot{z}_{\text{in}}$ and $\dot{z}_{\text{out}}$ respectively. $\dot{z}_{\text{out}}$ is needed for a reduction of the sinkage as the wheel travels onto fresh soil.

The increase of the sinkage is dependent on the longitudinal slip velocity of the wheel

$$v_s = \omega r - v_{t,x} \tag{8}$$

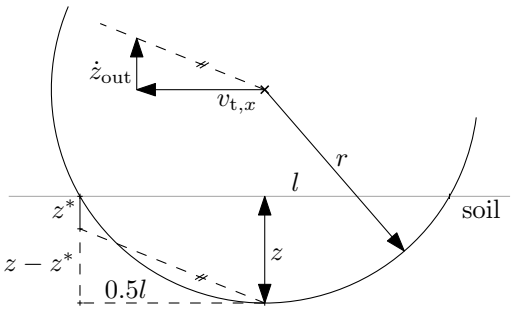

Fig. 2: Visualization of the outward dynamic sinkage calculation

with the turn rate ω and longitudinal velocity $v_{\text{t},x}$. The slip-sinkage is then calculated as

$$\dot{z}_{\text{in}} = k_{\text{s,max}} \left(\frac{\max\left(k_{\text{s},0} - z, 0\right)}{k_{\text{s},0}} \right)^{k_{\text{s,exp}}} |v_{\text{s}}| \tag{9}$$

where the slip-sinkage parameters k_{s} provide a sinkage-dependent scaling factor: The factor decreases with the sinkage where $k_{\text{s,max}}$ is the scaling factor at $z = 0$, $k_{\text{s},0}$ is the sinkage for which $\dot{z}_{\text{in}}$ reaches zero and $k_{\text{s,exp}}$ is the nonlinearity.

The total outward dynamic sinkage $\dot{z}_{\text{out}}$ is calculated dependent on the current sinkage z and an ideal sinkage

$$z^* = \left(\frac{mg}{k_{\text{c}}} \right)^{1/k_{\text{exp}}} \tag{10}$$

that represents the minimum needed sinkage to support the estimated mass m at the gravity g with spring constant k_{c} and exponent k_{exp}. As visualized in Fig. 2, it is assumed for $\dot{z}_{\text{out}}$ that the wheel climbs up a slope according to its minimum required sinkage z^* and the current contact patch length l. Through geometric similarity, the outward dynamic sinkage is calculated with the wheel forward velocity $v_{\text{t},x}$ and the contact patch length l as

$$\dot{z}_{\text{out}} = \min\left(\frac{(z - z^*)}{0.5l}, \tan\left(\phi_{\text{g}}\right) \right) |v_{\text{t},x}|. \tag{11}$$

Therein the climbing angle is limited by the modified internal friction angle ϕ_{g}, which is the internal friction angle ϕ of the soil corrected by the inclination of the soil plane in longitudinal wheel direction α,

$$\phi_{\text{g}} = \phi - \alpha. \tag{12}$$

The contact patch length l (cf. Fig. 2) is calculated with the radius r and the sinkage z as

$$\frac{l}{2} = \sqrt{2rz - z^2}. \tag{13}$$

Of the total outward dynamic sinkage from Eq. (11), the fraction that acts on the peak sinkage $\dot{z}_{\text{out,peak}}$ is implemented to decrease when the maximum possible force F_{peak} for the current peak sinkage z_{peak} is approached. This is achieved with a linear regularization within the elastic layer,

$$\dot{z}_{\text{out,peak}} = \min\left(\max\left(\frac{z_{\text{peak}} - z_{\text{eff}}}{d_{\text{el}}}, 0 \right), 1 \right) \dot{z}_{\text{out}} \tag{14}$$

The remaining outward dynamic sinkage acts on the slip-sinkage z_{s} according to

$$\dot{z}_{\text{out,s}} = \dot{z}_{\text{out}} - \dot{z}_{\text{out,peak}}. \tag{15}$$

3.1.4 Consolidation of the sinkage calculation

As described in Section 3.1.2, during an increase in plastic sinkage, the peak sinkage z_{peak} follows z_{eff}. When the effective sinkage falls below z_{peak}, the latter decreases with the outward dynamic sinkage $\dot{z}_{\text{out,peak}}$:

$$\dot{z}_{\text{peak}} = \begin{cases} \dot{z}_{\text{out,peak}} & \text{for} \quad z_{\text{eff}} < z_{\text{peak}} \\ \dot{z}_{\text{eff}} & \text{else.} \end{cases} \tag{16}$$

By using Eqs. (1), (2), (5) and (10) to (14) the outward dynamic peak sinkage $\dot{z}_{\text{out,peak}}$ can be computed as

$$\dot{z}_{\text{out,peak}} = \frac{k_{\text{el}}(z_{\text{peak}} + z_{\text{s}} - z)}{k_{\text{c}} z_{\text{peak}}^{(k_{\text{exp}})}} \min \left(\frac{\left(z - \left(\frac{k_{\text{c}}}{mg} \right)^{1/k_{\text{exp}}} \right)}{\sqrt{2rz - z^2}}, \tan(\phi - \alpha) \right) |v_{\text{t},x}|. \tag{17}$$

Therein z_{peak} and z_{s} are states; z, α and $|v_{\text{t},x}|$ are inputs; r, m, g, and ϕ are wheel/robot or soil parameters and all $k_{()}$ are model parameters.

Finally the slip-sinkage dynamics $\dot{z}_{\text{s}}$ is computed with $\dot{z}_{\text{out,s}}$ from Eqs. (14) and (15) and $\dot{z}_{\text{in}}$ from Eq. (9) as

$$\dot{z}_{\text{s}} = \dot{z}_{\text{in}} - \dot{z}_{\text{out,s}}. \tag{18}$$

3.2 Longitudinal force calculation

For the translational force, it is assumed that the maximum stress that the soil can bear is calculated according to MOHR-COULOMB [7] as

$$\tau_{\text{max}} = c + \frac{F_{\text{n}}}{A} \tan(\phi_{\text{g}}) \tag{19}$$

with the cohesion c, the contact patch area A and $F_{\text{n}}, \phi_{\text{g}}$ from Eqs. (7) and (12) respectively. Since the maximum shear stress is built up with shearing the material, JANOSI and HANAMOTO came up with an exponential expression as a function of the slip length j with the soil parameter k_{j} [7]:

$$\tau_{\text{j}} = \tau_{\text{max}} \left(1 - e^{\left(-j/k_{\text{j}} \right)} \right). \tag{20}$$

There are other models for the shear stress, e.g. for soil with cohesion or precompacted soil [7], yet all of them involve the shear length j.

Looking into the terramechanics in more detail, the j in Eq. (20) describes the shear length of the soil and hence is a state of the soil. For a correct modeling, the soil thus needs to be discretized in order to handle j as a state of individual soil patches. Since such a spatial discretization is avoided for performance reasons in this work, a different solution is required. Taking j as a state of the wheel, either discretized over the wheel rim or in one point only is not sensible since the shearing or loading is a soil behavior. To expound the conflict imagine a wheel traveling with constant speed and slip over a sand plane. If the integrated slip velocity of the wheel is used as j, the latter keeps rising and the maximum tangential shear stress τ_{max} is reached rather fast. Even for close to zero slip, j won't decrease anymore and thereby τ_{j} will stay high. However, since the wheel keeps reaching untouched soil when moving, the shear length j of this new soil has to be zero and for low slip this leads to a relatively low j over the contact patch.

This conflict of modeling the shear length j as a soil state without a spatial discretization of the soil is approached as follows in TerRA (cf. Fig. 3): The integral $\boldsymbol{j}_{\text{m}}$ of the slip velocity is computed in longitudinal (x) and lateral (y) wheel directions,

$$\boldsymbol{j}_{\text{m}} = \begin{bmatrix} j_{\text{m},x} \\ j_{\text{m},y} \end{bmatrix} = \begin{bmatrix} \boldsymbol{e}_x^{\top} \\ \boldsymbol{e}_y^{\top} \end{bmatrix} \int \underbrace{\boldsymbol{\omega}(t) \times \boldsymbol{r} + \boldsymbol{v}_{\text{t}}(t)}_{=\boldsymbol{v}_{\text{s}}} \mathrm{d}t, \tag{21}$$

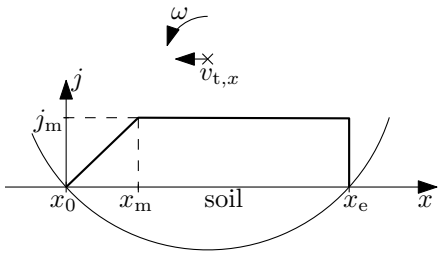

Fig. 3: Development of the slip length j over the wheel contact length x

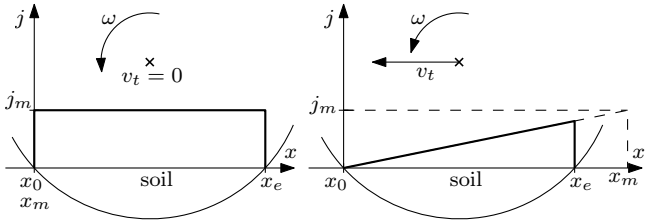

Fig. 4: Position x_m for zero (left) and high (right) translational velocity with the corresponding slip length graphs j

where r is the vector from the wheel hub to the wheel rim in the direction of the contact normal $\boldsymbol{n}$. Currently TerRA only computes forces in longitudinal direction, hence only the x-component of $\boldsymbol{j}_\mathrm{m}$ is considered and the coordinate in the index is omitted in the following: $j_x = j, j_{\mathrm{m},x} = j_\mathrm{m}$. j_m is taken as the current maximum slip length on the wheel contact patch and it is assumed that this shear length is built up linearly from the soil entry $x = 0$ to $x = x_\mathrm{m}$, which is computed with a PT1-filter as

$$x_\mathrm{m} = \mathrm{PT1}\left(\frac{v_{\mathrm{t},x}}{v_{\mathrm{s},x}} j_\mathrm{m}\right). \tag{22}$$

For $x > x_\mathrm{m}$, $j = j_\mathrm{m}$ stays constant at that maximum value as can be seen in Fig. 3. Note that this corresponds to a settled movement with constant slip and translational velocity as well as the simplification of a constant slip velocity over the contact patch.

In Fig. 4, the slip length graph for zero (left) and relatively high (right) translational velocity can be seen. Since the resulting tangential force corresponds to the integral over the slip length between soil entry x_0 and exit x_e, it shrinks with high translational velocities. This makes sense when considering that a lot of new soil comes in touch with the wheel and needs to be loaded, i.e. the slip length needs to be built up. As in the right case in Fig. 4, for high translational velocities it is possible that the maximum integrated slip length j_m cannot even be reached within the contact length x_e.

Using Eq. (20) with the described approach for the slip length and assuming constant stress over the wheel width w, the traction Force can be formulated similar to [7] as

$$\begin{aligned} F_\mathrm{tr} &= \int_{x_0}^{x_\mathrm{e}} \int_{-w/2}^{w/2} \tau_\mathrm{max}\left(1 - e^{-\left(j(t)/k_\mathrm{j}\right)}\right) \mathrm{d}y\,\mathrm{d}x \\ &= w\tau_\mathrm{max} \begin{cases} \left[x_\mathrm{e} + x_\mathrm{m}\dfrac{k_\mathrm{j}}{j_\mathrm{m}}\left(e^{-(j_\mathrm{m}x_\mathrm{e})/(x_\mathrm{m}k_\mathrm{j})} - 1\right)\right] & \text{for } x_\mathrm{m} > x_\mathrm{e} \\ \left[x_\mathrm{e}\left(1 - e^{-\left(j_\mathrm{m}/k_\mathrm{j}\right)}\right) + x_\mathrm{m}\left(\dfrac{k_\mathrm{j}}{j_\mathrm{m}}\left(e^{-\left(j_\mathrm{m}/k_\mathrm{j}\right)} - 1\right) - e^{-\left(j_\mathrm{m}/k_\mathrm{j}\right)}\right)\right] & \text{else.} \end{cases} \end{aligned} \tag{23}$$

Additionally, the wheel sinkage leads to a maximum soil resistance force F_res. This force is approximated with the formula of the passive earth pressure of a smooth, vertical surface that penetrates the soil to depth z and is pushed through the soil [19] as

$$F_\mathrm{res} = 0.5\rho g z^2 \left(\tan^2\left(\frac{\pi}{4} + \frac{\phi}{2}\right)\right) + 2cz\tan\left(\frac{\pi}{4} + \frac{\phi}{2}\right) \tag{24}$$

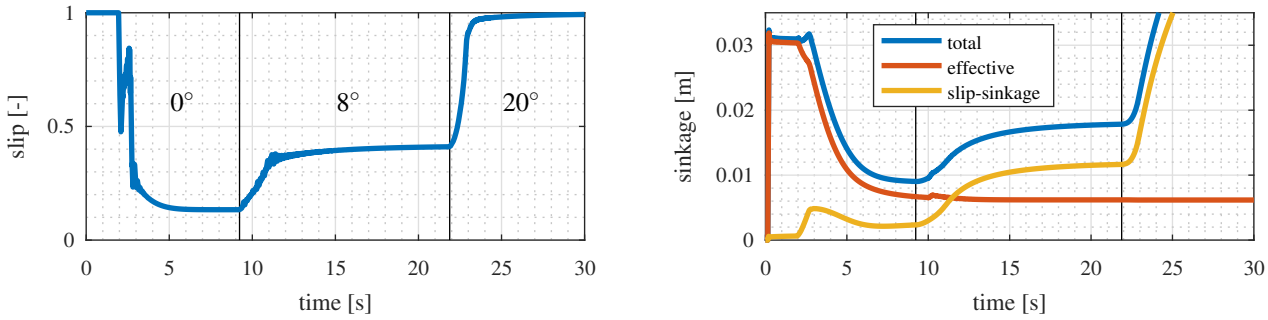

Fig. 5: Wheel slip (left) and sinkages (right) for a single wheel traveling on different slopes

For the final tangential force F_t, the traction force from Eq. (23) is regularized with a hyperbolic tangent around zero slip velocity for numerical smoothness. The resistance force from Eq. (24) should only oppose translational velocity v_t. To ensure numerical stability and prevent a residual steady-state error, a limited PI-controller with the maximum resistance force F_res as its limit is used:

$$\tilde{F}_\mathrm{res} = k_\mathrm{P}\left(v_\mathrm{t}F_\mathrm{res} + k_\mathrm{I}\int\left(v_\mathrm{t}F_\mathrm{res} - \frac{1}{k_\mathrm{P}k_\mathrm{awu}}\Delta_\mathrm{lim}\right)\mathrm{d}t\right), \tag{25}$$

$$F_\mathrm{t} = F_\mathrm{tr}\tanh\left(-\frac{v_\mathrm{s}}{v_\mathrm{thresh}}\right) + \begin{cases} F_\mathrm{res} & \text{for } \tilde{F}_\mathrm{res} > F_\mathrm{res} \\ -F_\mathrm{res} & \text{for } \tilde{F}_\mathrm{res} < -F_\mathrm{res} \\ \tilde{F}_\mathrm{res} & \text{else} \end{cases}. \tag{26}$$

Therein Δ_lim is the overrun of the minimum or maximum $-F_\mathrm{res}$ or F_res and k_awu is the anti-windup factor which is set to 1 within this work.

The effect of grousers that is e.g. described in [11] is not explicitly considered here. According to [15], the average effect of grousers can be approximated by increasing the equivalent radius of the wheel and entry and exit angles for the simulation. Additionally, the variation in the traction force due to grousers can be modeled as oscillations according to [20]. For the TerRA model, the average effect of grousers is already implicitly considered through the fitting process, the oscillation is not considered yet but could be added similar as in [20] in further work if needed.

4 Model evaluation

A verification of the qualitative model behavior with the requirements that were stated in Section 2 is shown in Section 4.1 before presenting a systematic procedure to adjust the model parameters to fit high fidelity simulation or experimental data in Section 4.2.

4.1 Qualitative requirement verification

To start the evaluation, the fulfillment of the requirements from Section 2 is checked with a simple single wheel scenario (see Table 1 for the wheel and model parameters). The wheel drops on flat ground at $t = 0\,\mathrm{s}$ and subsequently starts driving at $t = 2\,\mathrm{s}$ with a constant angular velocity of $0.5\,\mathrm{rad\,s^{-1}}$ and a constant drawbar pull force of $10\,\mathrm{N}$, i.e. a force that counteracts the longitudinal movement. At $t \approx 9\,\mathrm{s}$ and $t \approx 22\,\mathrm{s}$, the wheel hits a 8° and a 20° slope, respectively (cf. Fig. 5). The wheel movement is free in its vertical and longitudinal direction.

In the following detailed description of the result that are plotted in Fig. 5, key-words of the requirements from Section 2 are *emphasized*.

In the beginning the wheel drops into the sand, resulting in a *plastic sinkage* which can be seen as part of the red line in the right plot of Fig. 5 and remains until the wheel starts moving translationally from $\approx 2.5\,\mathrm{s}$ on. Shortly before, at $t = 2\,\mathrm{s}$, the wheel starts rotating, however, due to the *slip and traction force* relation the latter is not built

Wheel	
radius (w/o grouser)	0.125 m
width	0.15 m
number of grousers	12
grouser height	7.5 mm
mass	10 kg

TerRA parameters	
k_c	$3.6 \times 10^4\,\mathrm{N\,m^{-1}}$
k_{exp}	1.17
k_d	0.05
k_{el}	$5 \times 10^5\,\mathrm{N\,m^{-1}}$
$k_{s,0}$	0.15 m
$k_{s,exp}$	5
$k_{s,max}$	0.5

Tab. 1: Wheel and model parameters of the qualitative single wheel test

up immediately. This leads to the wheel only slowly accelerating between $t = 2\,\mathrm{s} - 5\,\mathrm{s}$ which in turn results in a initially high but decreasing slip (cf. left plot in Fig. 5). The *slip-sinkage* (cf. yellow line in the right plot in Fig. 5) increases from $t = 2\,\mathrm{s}$ to $t = 3\,\mathrm{s}$. Since the wheel can overcome its *resistance force* with a sufficient traction force being developed, it drives out of its imprint and both the *slip-sinkage* and the effective sinkage (its plastic part to be more precise) decrease from $t = 3\,\mathrm{s}$ to $t = 9\,\mathrm{s}$.

When hitting the first slope at $t \approx 9\,\mathrm{s}$, a higher traction force is needed which - according to the relation of *slip and traction force* - can only be achieved with higher slip. This in turn increases the *slip-sinkage* as can clearly be seen in the right plot of Fig. 5 until a *convergence* in slip and sinkage is reached. A similar behavior can be observed from $t \approx 22\,\mathrm{s}$ on when the wheel hits the 20° slope with the difference, that the amount of slip needed to produce the necessary traction force leads to a large *slip-sinkage*. This sinkage comes with a *resistance force* that cannot be overcome anymore and the wheel gets stuck which can be seen by means of the slip value approaching 100 % in the left plot of Fig. 5.

The described simulation of one wheel with TerRA runs roughly 100-times *faster than real-time* with a step size of 1 ms on a standard office computer, i.e. the evaluation of one simulation step including the multibody solver takes about $10^{-5}\,\mathrm{s}$.

4.2 Setting the model parameters

As described in Section 2, TerRA is supposed to be fitted to results of either validated more complex models or of single wheel tests. For this work, the DLR Soil Contact Model [22] which features force/torque as well as soil flow calculation enabled by a 2,5-dimensional soil discretization is used and referred to as the *reference* results in the following.

To fit the various TerRA parameters, a systematic approach using different scenarios and evaluation criteria as well as the Modelica Optimization Library [23] is developed. The use of multiple optimization runs to tune the model modules individually helps the optimization algorithm to not get stuck in local minima. The different scenarios with the respective tuners and optimization criteria are summarized in the following.

4.2.1 Drop test

For finding the parameters of the nonlinear spring and the linear damping factor in Eqs. (2) and (6), a drop test of the wheel from different heights is performed.

The scenario is a flat surface with three wheels identical to the one in Table 1 that are initialized at heights of $z_0 = \{1.1, 2, 3\}r$ and fall down on the ground due to the gravitational force. As a result of the different heights, different impact energy causes different plastic sinkages as can be seen in the result plot in Fig. 6. After a short settling period, the wheels remain stationary at a certain sinkage z which is compared to the reference result for the evaluation criterion

$$z_{\mathrm{err,rel}} = \frac{z - z_{\mathrm{ref}}}{z_{\mathrm{ref}}}. \tag{27}$$

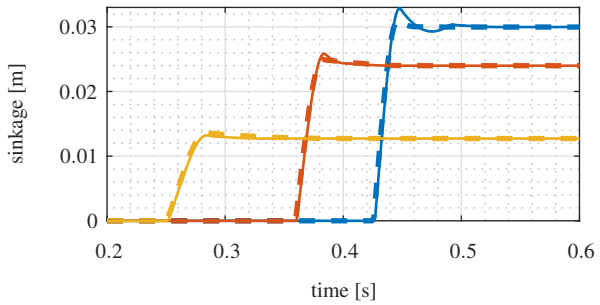

Fig. 6: Sinkage of three identical wheels that drop onto the ground from $z_0 = 3r$, $z_0 = 2r$, $z_0 = 1.1r$ (blue, red, yellow). The dashed line is the reference and the solid one the TerRA result

parameter	fitted value
k_c	$8.01 \times 10^5\,\mathrm{N\,m^{-1}}$
k_{exp}	1.71
k_d	1.09×10^{-2}
k_{el}	$7.98 \times 10^5\,\mathrm{N\,m^{-1}}$

z_0	$z_{err,rel}$
$1.1r$	0.07 %
$2r$	0.11 %
$3r$	0.07 %

Tab. 2: Results of fitting the drop test: final model parameters for TerRA (left) and resulting settled relative sinkage error (right).

To make sure that the steady state is compared, the sinkage is averaged after waiting for a settling time of 2 s over a period of 0.5 s.

The model parameters that are found with this scenario are the spring constant k_c, the exponent k_{exp}, the elastic layer stiffness k_{el} and the damping factor k_d, cf. Eqs. (2) and (6). To ease the convergence of the optimization algorithm, a base spring constant $\bar{k}_c$ is used as a tuner instead of using k_c directly such that

$$k_c = z_{base}^{(1-k_{exp})} \bar{k}_c. \tag{28}$$

This makes the force at the base sinkage z_{base} independent of the spring exponent k_{exp}, i.e. the interdependency of the parameters is reduced. The base wheel is chosen arbitrarily from the set of wheels in the scenario.

The optimization consists of two independent optimization runs with the sequential quadratic program (SQP) algorithm of the Modelica Optimization Library [23]. In the first run only the chosen base wheel sinkage is taken as a criterion and the base spring constant $\bar{k}_c$ is the sole tuner. With that first run, a good initial guess for the main optimization run can be found. The second run features the minimization of the sum of squares of all sinkage errors by tuning the base spring constant $\bar{k}_c$, the spring exponent k_{exp}, the elastic layer stiffness k_{el} and the damping factor k_d.

The result of this fitting scenario can be seen in Fig. 6, where the dashed line is the SCM reference sinkage and the solid line the one of the final fitted TerRA model. The different colors represent the three drop heights: blue is $z_0 = 3r$, red is $z_0 = 2r$ and yellow is $z_0 = 1.1r$. The steady state sinkage error is below 1 % (cf. Table 2 and the transient behavior (which is not subject to the optimization) is similar. TerRA shows a bit more elastic sinkage component, especially for the impact with the most energy (blue line in Fig. 6) which mostly results from a nonlinear damping in the reference model SCM that does not exist in TerRA.

4.2.2 Drawbar pull test

The so-called *Drawbar Pull (DBP)* test is a single wheel test where the turn and longitudinal velocity - and thereby the slip - are fixed and the wheel is free in its movement in the vertical direction. For emulating a certain system weight, a fixed normal force is applied by attaching a mass to the wheel. The performance of wheels is then evaluated by means of the longitudinal force - commonly referred to as DBP force - for different fixed slip values.

For this work, the DBP test is performed in simulation with the DLR soil contact model. The wheel from

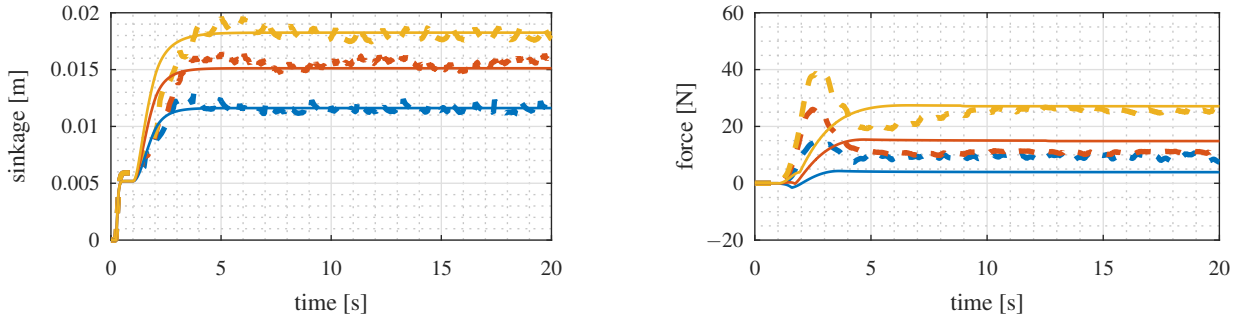

(a) Wheel sinkages

(b) Drawbar pull force

Fig. 7: Drawbar pull results, reference model results are plotted as dashed lines, TerRA results as solid lines.

slip	sinkage error $z_{\mathrm{err,rel}}$	DBP force error $F_{\mathrm{err,rel}}$
20 %	1.0 %	58.2 %
40 %	2.5 %	34.5 %
60 %	1.4 %	5.5 %

Tab. 3: Resulting errors of the average settled values for the drawbar pull test.

Table 1 and slip values of 20 %, 40 % and 60 % are used to fit the dynamic sinkage and force behavior to the reference.

The model parameters to be found with this test are the dynamic sinkage parameters $k_{\mathrm{s,max}}, k_{\mathrm{s,0}}$ and $k_{\mathrm{s,exp}}$ as well as the shear parameter k_{j}, cf. Eqs. (9) and (20). Similar to Section 4.2.1 a base maximum dynamic sinkage parameter $\bar{k}_{\mathrm{s,max}}$ is introduced with

$$k_{\mathrm{s,max}} = \left(\frac{k_{\mathrm{s,0}} - z_{\mathrm{base}}}{k_{\mathrm{s,0}}} \right)^{1-k_{\mathrm{s,exp}}} \bar{k}_{\mathrm{s,max}} \tag{29}$$

and used as tuner instead of $k_{\mathrm{s,max}}$ to reduce the interdependency of the model parameters. The spring and damping parameters that were found in Section 4.2.1 remain unchanged in this scenario.

The fitting of the DBP scenario consists of three independent optimization runs. Similar to Section 4.2.1, to make sure that only the settled values are compared, the average over half a wheel rotation is taken only after waiting for one full wheel rotation. Similar to the previous paragraph, two steps are pursued for the dynamic sinkage to first find a good start point for the full optimization and the evaluation criterion is again the relative sinkage error from Eq. (27). The sinkage of the arbitrarily chosen base wheel is fitted by finding only the optimal base maximum dynamic sinkage parameter $\bar{k}_{\mathrm{s,max}}$ while keeping all other parameters constant. Taking the found value as a starting point, all dynamic sinkage parameters are tuned by minimizing the sum of squares of all sinkage errors. The result of fitting the sinkage can be seen in Fig. 7a and quantitatively in Table 3: A small steady state error of 2.5 % and smaller is achieved. The transient behavior shows similarity, however the dynamic sinkage is developed faster in TerRA compared to the reference.

In a last run, the sum of squares of the three wheels' relative longitudinal force errors

$$F_{\mathrm{err,rel}} = \frac{F - F_{\mathrm{ref}}}{F_{\mathrm{ref}}} \tag{30}$$

are minimized by tuning the shear parameter k_{j}. The transient behavior can be seen in Fig. 7b and the quantitative fitting errors in Table 3. It can be seen that it is not possible to tune TerRA to the DBP force of the reference model, which results in errors of almost 60% and the transient behavior showing considerable differences. This is due to k_{j} being the only tuning parameter for the longitudinal force in the current implementation, thus the level of the DBP can be adjusted but not the gradient for different slip values. However, since the used DLR Soil Contact Model is

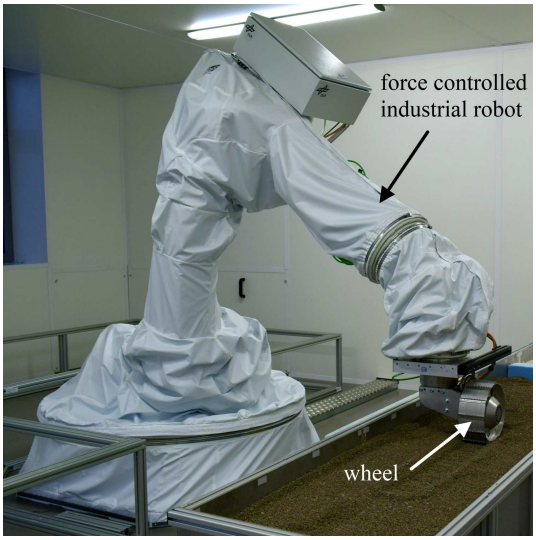

Fig. 8: The Terramechanics Robotics Locomotion Lab (TROLL)

not yet validated on a force level, lab experiments in the new Terramechanics Robotics Locomotion Lab (TROLL), see Fig. 8 [21], should be performed. It must be investigated whether the model behavior of TerRA without further parameters is good enough to reach the desired result quality or if further development - potentially with additional parameters - is required. Possible adjustments involve the computation of the length where the shear length is fully build up x_m from Eq. (22) and the computation of the resistance force from Eq. (24).

5 Conclusions

A novel empirical one-point terramechanics model for the normal and longitudinal force simulation of wheeled locomotion was developed with a special focus on fast computation. After a brief overview of existing models, effects that shall be covered and additional requirements were stated.

The model was presented in detail and therefore separated into normal and longitudinal direction. The normal force calculation features an elasto-plastic behavior with a nonlinear spring characteristic and linear damping. Additionally, a novel form of including dynamic sinkage was derived that features slip-sinkage and the possibility of driving out of a generated imprint without soil discretization. For the translational force calculation a combination of slip-length dependent traction force and sinkage dependent soil resistance force was presented. Lowering of traction force for untouched, unsheared soil getting under the wheel while moving translationally, was enabled by a novel approach based on slip and translational velocity.

To verify the fulfillment of the requirements, a qualitative one wheel scenario was shown and the results were described in detail. A procedure for tuning the model parameters to a higher fidelity model or experiment data that is based on optimization was finally presented and the possible fitting quality was shown. The static and dynamic sinkage fit was found to be of good quality whereas the longitudinal force calculation with only one model parameter has shown to be not sufficient for the specific reference data that was used.

Future work needs to be directed to the verification of the inter- and extrapolation capabilities of TerRA with scenarios that differ from those that have been used for tuning. Tests in the new Terramechanics Robotics Locomotion Lab should be made to create experimental reference data. For the further development, special focus must be put onto the investigation of the shown shortcomings of the longitudinal force calculation. Furthermore a lateral force as well as steering torque computation shall be developed for performing full system simulations with TerRA. Finally the existing parameters shall be checked for dependency and relation to independently measurable or physical parameters.

References

[1] R. E. Arvidson *et al.*, "Spirit mars rover mission: Overview and selected results from the northern home plate winter haven to the side of scamander crater," *Journal of Geophysical Research: Planets*, vol. 115, no. E7, 2010.

[2] ——, "Opportunity mars rover mission: Overview and selected results from purgatory ripple to traverses to endeavour crater," *Journal of Geophysical Research: Planets*, vol. 116, no. E7, 2011.

[3] ——, "Mars science laboratory curiosity rover terramechanics initial results," in *44th Lunar and Planetary Science Conference, held March 18-22, 2013 in The Woodlands, Texas. LPI Contribution No. 1719*, 2012, p. 1193.

[4] M. Maimone, Y. Cheng, and L. Matthies, "Two years of visual odometry on the mars exploration rovers," *Journal of Field Robotics*, vol. 24, no. 3, pp. 169–186, 2007.

[5] R. E. Arvidson *et al.*, "Mars science laboratory curiosity rover megaripple crossings up to sol 710 in gale crater," *Journal of Field Robotics*, vol. 34, no. 3, pp. 495–518, 2017.

[6] R. Lichtenheldt, S. Barthelmes, F. Buse, and M. Hellerer, "Wheel-ground modeling in planetary exploration: From unified simulation frameworks towards heterogeneous, multi-tier wheel ground contact simulation," in *Multibody Dynamics: Computational Methods and Applications*, J. M. Font-Llagunes, Ed. Springer International Publishing, 2016, pp. 165–192.

[7] J. Y. Wong, *Theory of Ground Vehicles*, 4th ed. Hoboken, New Jersey, USA: John Wiley & Sons, Inc., 2008.

[8] L. Ding, Z. Deng, H. Gao, K. Nagatani, and K. Yoshida, "Planetary rovers' wheel—soil interaction mechanics: new challenges and applications for wheeled mobile robots," *Intelligent Service Robotics*, vol. 4, no. 1, pp. 17–38, 2011.

[9] G. Meirion-Griffith and M. Spenko, "A modified pressure–sinkage model for small, rigid wheels on deformable terrains," *Journal of Terramechanics*, vol. 48, no. 2, pp. 149–155, 2011.

[10] L. Ding, H.-b. Gao, Z.-q. Deng, and J.-g. Tao, "Wheel slip-sinkage and its prediction model of lunar rover," *Journal of Central South University of Technology*, vol. 17, pp. 129–135, 2010.

[11] F. Zhou *et al.*, "Simulations of mars rover traverses," *Journal of Field Robotics*, vol. 31, no. 1, pp. 141–160, 2014.

[12] H. Gao *et al.*, "Longitudinal skid model for wheels of planetary exploration rovers based on terramechanics," *Journal of Terramechanics*, vol. 50, no. 5, pp. 327–343, 2013.

[13] Z. Jia, W. Smith, and H. Peng, "Terramechanics-based wheel–terrain interaction model and its applications to off-road wheeled mobile robots," *Robotica*, vol. 30, no. 3, pp. 491–503, 2012.

[14] L. Ding, H. Gao, Y. Li, G. Li, and Z. Deng, "Improved explicit-form equations for estimating dynamic wheel sinkage and compaction resistance on deformable terrain," *Mechanism and Machine Theory*, vol. 86, pp. 235–264, 2015.

[15] Z. Jia, W. Smith, and H. Peng, "Fast analytical models of wheeled locomotion in deformable terrain for mobile robots," *Robotica*, vol. 31, no. 01, pp. 35–53, 2013.

[16] W. Petersen, "A volumetric contact model for planetary rover wheel/soil interaction," Ph.D. dissertation, University of Waterloo, 2013.

[17] A. Azimi, J. Kövecses, and J. Angeles, "Wheel–soil interaction model for rover simulation and analysis using elasto-plasticity theory," *IEEE Transactions on robotics*, vol. 29, no. 5, pp. 1271–1288, 2013.

[18] R. Lichtenheldt and O. Krömer, "Soil modeling for InSight's HP^3-Mole: From highly accurate particle-based towards fast empirical models," in *ASCE Earth and Space 2016*, ser. Earth & Space. ASCE, 2016.

[19] K. Terzaghi, R. B. Peck, and G. Mesri, *Soil mechanics in engineering practice*. John Wiley & Sons, 1996.

[20] R. Irani, R. Bauer, and A. Warkentin, "A dynamic terramechanic model for small lightweight vehicles with rigid wheels and grousers operating in sandy soil," *Journal of Terramechanics*, vol. 48, no. 4, pp. 307–318, 2011.

[21] F. Buse, T. Bellmann, and R. Lichtenheldt, "The terramechanics robotics locomotion lab," in *Proceedings of the 14th International Symposium on Artificial Intelligence, Robotics and Automation in Space (i-SAIRAS)*, 2018.

[22] F. Buse, "Using superposition of local soil flow fields to improve soil deformation in the DLR soil contact model - SCM," in *Proceedings of the 5th Joint International Conference on Multibody System Dynamics (IMSD)*, 2018.

[23] A. Pfeiffer, "Optimization library for interactive multi-criteria optimization tasks," in *Proceedings of the 9th International Modelica Conference*, 2012, pp. 669–680.